OPEN ACCESS Freely available online

PLOS ONE

Molecular Probe Dynamics Reveals Suppression of Ice-Like Regions in Strongly Confined Supercooled Water

Debamalya Banerjee[1], Shrivalli N. Bhat[1], Subray V. Bhat[1]*, Dino Leporini[2,3]*

1 Department of Physics, Indian Institute of Science, Bangalore, India, **2** Dipartimento di Fisica "Enrico Fermi," Università di Pisa, Pisa, Italy, **3** Instituto per i Processi Chimico-Fisici–Consiglio Nazionale delle Ricerche, UoS Pisa, Pisa, Italy

Abstract

The structure of the hydrogen bond network is a key element for understanding water's thermodynamic and kinetic anomalies. While ambient water is strongly believed to be a uniform, continuous hydrogen-bonded liquid, there is growing consensus that supercooled water is better described in terms of distinct domains with either a low-density ice-like structure or a high-density disordered one. We evidenced two distinct rotational mobilities of probe molecules in interstitial supercooled water of polycrystalline ice [Banerjee D, et al. (2009) ESR evidence for 2 coexisting liquid phases in deeply supercooled bulk water. Proc Natl Acad Sci USA 106: 11448–11453]. Here we show that, by increasing the confinement of interstitial water, the mobility of probe molecules, surprisingly, increases. We argue that loose confinement allows the presence of ice-like regions in supercooled water, whereas a tighter confinement yields the suppression of this ordered fraction and leads to higher fluidity. Compelling evidence of the presence of ice-like regions is provided by the probe orientational entropy barrier which is set, through hydrogen bonding, by the configuration of the surrounding water molecules and yields a direct measure of the configurational entropy of the same. We find that, under loose confinement of supercooled water, the entropy barrier surmounted by the slower probe fraction exceeds that of equilibrium water by the melting entropy of ice, whereas no increase of the barrier is observed under stronger confinement. The lower limit of metastability of supercooled water is discussed.

Citation: Banerjee D, Bhat SN, Bhat SV, Leporini D (2012) Molecular Probe Dynamics Reveals Suppression of Ice-Like Regions in Strongly Confined Supercooled Water. PLoS ONE 7(9): e44382. doi:10.1371/journal.pone.0044382

Editor: Chandra Verma, Bioinformatics Institute, Singapore

Received January 17, 2012; **Accepted** August 6, 2012; **Published** September 26, 2012

Funding: The work was financially supported by the Indian National Science Academy and the University of Pisa. The funders had no role in study design, data collection and analysis, decision to publish, or preparation of the manuscript.

Competing Interests: The authors have declared that no competing interests exist.

* E-mail: svbhat@physics.iisc.ernet.in (SVB); dino.leporini@df.unipi.it (DL)

Introduction

Several water anomalies with deep implications in biology, atmospheric phenomena, geology, and food technology are rooted in the supercooled liquid state [1–6]. While there is wide consensus, with some controversy [7,8], that water near ambient conditions is a uniform, continuous liquid [9], our understanding of water in the supercooled state below the freezing point is still widely debated.

Models of supercooled water: an overview

The different viewpoints on supercooled water can be partitioned into two broad classes: mixture/interstitial models and distorted hydrogen bond or "continuum" models [10]. Mixture models consider that liquid water is composed of a small number of distinct components where molecules are surrounded by immediate neighborhoods with distinguishable structures. Whiting was the first to consider in 1884 liquid water as a mixture of a solid ice-like component and a normal liquid [11]. Later, mixture models with sharp distinction between "intact" and "broken" hydrogen bond (HB) were reported [12,13]. However, the difficulty in specifying a few distinct states of liquid water motivated the growth of the continuum models. In this framework, first developed by Bernal and Fowler in 1933 [14] and Pople in 1951 [15], the picture of water structure is considered as a continuous distribution of approximately tetrahedral environments, corresponding to different degrees of distortion of the hydrogen bond (HB) ranging from strong HB's such as those in ice to highly distorted or even broken HB's [10]. The tendency to aggregation of unstrained ice-like polyhedra was also noted [1,16] with increasing correlation length of the structure fluctuations [17]. An important new step about the structural aspects of water was the experimental observation of the phase transition between two different forms of amorphous ice by Mishima and coworkers [18]. The two amorphous ice phases were incorporated in the picture of the metastable and stable water by the liquid-liquid critical point (LLCP) scenario where [19]: i) liquid water displays polymorphism, i.e. it exists in two different phases, a highly-disordered high-density liquid (HDL), entropically favored, and a low density liquid (LDL) with local ice-like tetrahedral order, energetically favored, ii) the first-order LDL-HDL phase transition line terminates at a liquid-liquid critical point in the supercooled region. The LLCP scenario may be seen as a modern development of the mixture models. The universality of liquid-liquid phase transitions was argued in terms of two competing orderings, i.e. density ordering and bond ordering [20] leading in water to the formation of a rather stable ice-like locally favored structure in a sea of disordered normal-liquid structures [21]. To date, in addition to LLCP, three other separate thermodynamic scenarios have been proposed, i.e. the stability limit scenario [22], the singularity-free scenario [23,24] and the critical-point free scenario

[4]. It has been recently shown that LLCP scenario and the three other ones, including models that can reproduce more than one scenario [21,25,26], can be accounted for by one general scheme which predicts a LLCP at positive pressure [27].

Current evidence of ice-like regions in supercooled water

The above discussion pointed out that regions of ice-like supercooled water are expected by mixture models of water [19,21], as well as by the consideration of the strain energy of isolated elementary structural unit of hexagonal ice in a locale of strained and broken HB's [1,16].

In parallel with several numerical studies, e.g. [17,19,23,25–31], support to an increase in tetrahedrality and the presence of two different structural motifs in supercooled water is provided by a number of experimental findings. This includes discontinuities in the melting curve of high-pressure ice [32], changes in the local structure of both ambient water under pressure [33] and supercooled water confined in nanopores [34] or protein crystals [35], vibrational properties of nanoconfined water [36], enhanced density fluctuations in supercooled [37] and, controversially [8,9], ambient water [7], bimodal mobility of guest molecules in interstitial supercooled water of polycrystalline ice [38], density hysteresis of nanoconfined heavy water [39]. However, consensus is not complete, e.g. on the existence of only two forms of amorphous water [40], the polyamorphism of liquid water [41], or the differences between bulk and confined water [4–6,42–44].

Water confinement in polycrystalline ice

At ambient pressure the supercooled regime of water ranges between the glass transition temperature $T_g \simeq 136K$ [3,45,46] and the melting temperature T_m. Above T_g water transforms into a highly viscous fluid [3] crystallizing at $T_X \sim 150K$. Since bulk water can be supercooled down to the homogeneous nucleation temperature $T_H \sim 235K$, the region between T_X and T_H has been regarded as a region where liquid water is absent ("no man's land", NML [2]). Nonetheless, the coexistence of crystals and deeply supercooled liquids was suspected already one century ago for bulk systems [47] (see also ref.[48]). More recently, the coexistence of ice and supercooled water was predicted by Nye and Frank [49,50] and reported by experiments [51,52], especially in the temperature range $140-210$ K [53–61], and by simulations in NML [29,62]. Under suitable conditions the amount of liquid water in polycrystalline ice is not negligible. In the devitrification of vapor deposited solid only about 30% of the material is transformed into cubic crystals of about $10-15$ nm [55] and the remaining part has been identified as liquid [56]. Furthermore, simulations evidence still 15%–20% of liquid water between nanometer-sized ice crystals in NML [62].

In polycrystalline ice liquid water is localized where three grain meet in channels, or veins, that generally extend along the whole length of the grain edge. Four veins meet in a node (pocket) at a four-grain intersection, thereby forming a sponge-like, interconnected network of veins known as the vein system. The network was evidenced by experiments [51,52,61,63] and simulations [29] and serve as interstitial reservoirs for impurities [51,52,58,60,61,63,65–69]. The vein width δ decreases with the temperature from the micrometer range very close to T_m [51,52,63] down to dozens of nanometers at about 190 K [61].

Dimensional arguments lead to the conclusion that the volume fraction (f) of water with respect to ice in the vein system has the expression [59]:

$$f = \alpha_v \left(\frac{\delta}{a}\right)^2 + \alpha_p \left(\frac{\delta}{a}\right)^3 \quad (1)$$

a is the average grain diameter, α_v and α_p are dimensionless quantities depending on the geometry of the grain. The square term was derived by Frank [49,70] who found $\alpha_v = 6\pi\sqrt{2}/4 \sim 6.7$ (the extra factor of four with respect to his result follows by considering both δ and a as diameters). The cubic term is the correction due to the finite volume of the pockets [59]. It was predicted [49,50,58,59] and confirmed by experiments [51,52] that the vein size δ is determined by the thermodynamic properties like the relative surface energies of solid-solid and solid-liquid interfaces as well as by the temperature. Differently, the grain size is controlled by the thermal history. This aspect is discussed in detail in the next section.

Thermal protocols for varying polycrystallinity

The experiments show that the size of the ice grains decreases by increasing the cooling rate [61,64,71]. The crystallization starting in the course of slow entrance into the supercooled region above T_H leads to macroscopic grains in the millimeter range [51]. Instead, much higher polycrystallinity is found in the ice formation following the devitrification of amorphous water above T_g leading to small grains of about $10-15$ nm for thin films [55] or 40 nm for thicker films [53]. This is in harmony with thermodynamic arguments leading to the conclusion that cubic ice particles with size of a few nanometers can coexist with water droplets of about the same size at temperatures in the $150-180$ K range [60].

From the above discussion it follows that the liquid fraction in polycrystalline ice close to T_m is quite small. Indeed, by taking $\delta \sim 100\mu$m and $a \sim 10$ mm [51], one yields from Eq. 1 $f \sim 6.7(\delta/a)^2 \sim 6.7(10^{-4}/10^{-2})^2 \sim 6.7 \cdot 10^{-4}$, to be compared with the estimate $f \lesssim 10^{-3}$ close to T_m [49]. Distinctly, after quench cooling close to T_g one has $\delta \sim 40$ nm [61] and $a \sim 40$ nm [53,55]. This is consistent with the experimental finding $f \sim 0.7$ [56], and the anticipated coexistence of nanograins and nanodroplets of about the same size in the $150-180$ K range [60].

One may resort to the different character of the vein size (controlled by the thermodynamics) and the grain size (controlled by the thermal history) to control the degree of confinement of the liquid fraction in ice/water mixtures. Consider two ice-water mixtures with different polycrystallinity and equal temperature $T \gtrsim T_g$, one resulting from the devitrification by rewarming previously quench-cooled water (quenched-rewarmed or QRW protocol), another with ice nucleated and grown close to T_m and then slowly cooled down to T (slowly cooled or SC protocol), see Fig. 1. The mixtures have different grain size but very similar nanometric vein size. Thus, the devitrified sample with higher polycrystallinity exhibits a larger water fraction according to Eq. 1, which is less confined by the ice fraction due to the additional paths and intersections. Note that the exact temperature matching is not important to ensure very similar cross section of the vein δ in QRW and SC ice/water mixtures. In fact, a near inverse-square dependence of δ on the degree of supercooling is found [52]. This leads to a factor of ~ 2 increase in δ by rising the temperature from 130 K to 232 K.

It is worth noting that increasing the confinement of water close to a hydrophilic surface like ice is equivalent to a pressure (or density) increase [4,6,42]. This has the interesting consequence to unfavor the formation of unstrained, ice-like, hydrogen bond network in the confined water [42]. We also note that, according to recent simulations, strong confinement in hydrophobically

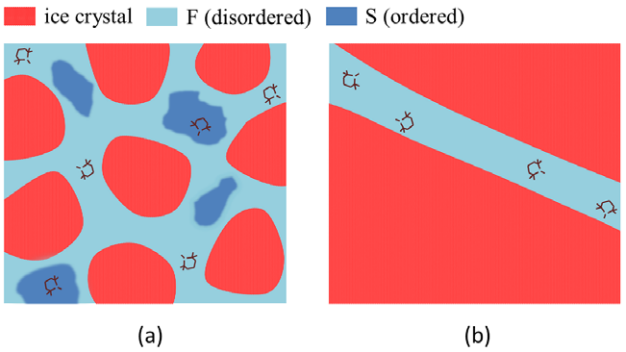

Figure 1. Two idealized ice/water mixtures with different polycrystallinity at $T \gtrsim T_g$. The scale of the pictures is the same. The two panels refer to the QRW (a) and the SC protocols (b), see text for details. The width of the liquid veins in the two mixtures is very similar and of the order of dozens of nanometers, whereas the size of the ice grains is $\sim 10^5$ times larger in SC mixtures. Augmenting of the polycrystallinity increases the water fraction f and reduces its confinement due to the additional paths and intersections. According to ref.[38] and the present study, ice-like patches (blue) with slow (S) mobility are included in the QRW liquid fraction. The patches are suppressed in the SC mixtures, leaving only the less ordered liquid fraction (light blue) with fast (F) mobility. The shape of the patches is unknown.
doi:10.1371/journal.pone.0044382.g001

nanoconfined water breaks cooperatively rearranging regions of 1 nm approximate size, facilitating the dynamics [72].

In a previous paper we reported evidence of two distinct rotational mobilities of probe molecules (spin probes) in interstitial supercooled water of polycrystalline ice [38]. The thermal protocol adopted in the sample preparation was the QRW protocol resulting, by devitrification, in a mixture of supercooled water and highly-polycristalline ice. It was speculated that the slow (S) and the fast (F) components of the probe molecules are trapped in the ice-like and the less ordered regions of the interstitial water, respectively (Fig. 1a). Here, we substantiate this claim by investigating the rotational mobility of the probe molecules in a water-ice mixture prepared by the SC protocol, i.e. by slowly cooling the sample from ambient conditions. The SC protocol yields ice with lower polycrystallinity than the QRW protocol and stronger water confinement (Fig. 1b).

The major conclusions of the study, which is presented and discussed below, are:

i) the S fraction of the spin probes is embedded in regions of QRW water with ice-like structure (fig. 1a),

ii) the ice-like environment is suppressed in the liquid fraction of SC ice/water mixtures (fig. 1b).

Results and Discussion

We studied the rotational motion of the polar nitroxide molecule TEMPOL (spin probe) in the interstitial liquid water of polycrystalline ice by using the Electron Spin Resonance (ESR) spectroscopy [74,75]. TEMPOL is a very stiff molecule and is coupled to water via hydrogen-bonds (HB), see Fig. 2 [73]. Due to the small size ($r_{TEMPOL} \sim 0.34 nm$ [38]), it is expected to perturb the water host in a limited way ($r_{H2O} \sim 0.14 nm$). The sample preparation is described in Materials and Methods together with details about the ESR spectroscopy of spin probes, see also ref.[38,75]. The guest molecule is expelled by the solid fraction and localizes in the interstices between the ice grains where the liquid water is trapped [38,45,58,60,66–69].

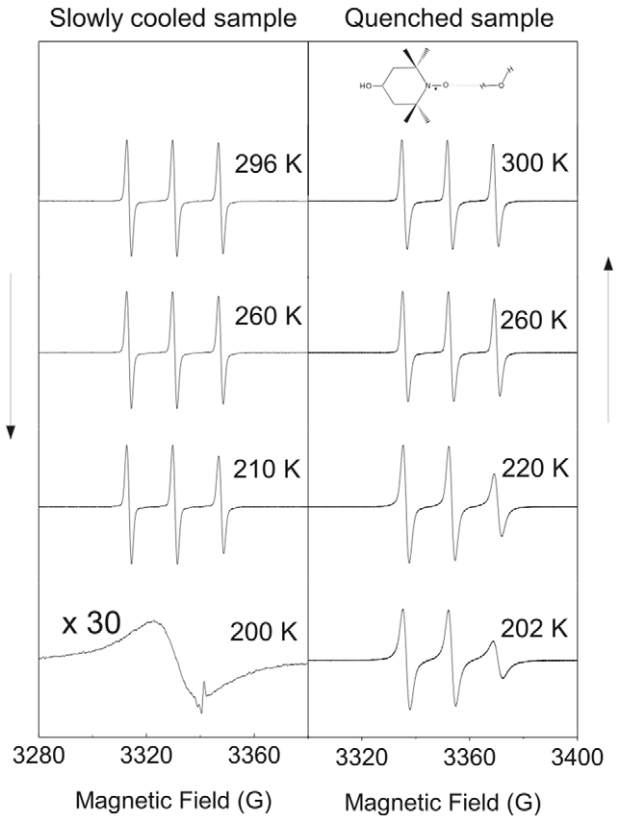

Figure 2. Structure and selected ESR lineshapes of the spin probe TEMPOL in water. Left: slowly cooled bulk water (SC protocol). Right: quenched and slowly re-heated bulk water at the indicated temperature (QRW protocol). The QRW sample contains ice with higher polycrystallinity. Note that the SC sample at 210 K exhibits narrower lines than QRW sample at 220 K, i.e. TEMPOL is rotating faster in SC water. The H-bonding of TEMPOL with water is shown in the top of the the right panel. Owing to the very weak ESR signal from TEMPOL in the SC sample at 200 K, a small spurious signal from the quartz capillary used is observed at 3340 G.
doi:10.1371/journal.pone.0044382.g002

Facilitated dynamics of TEMPOL in SC water

Fig. 2 presents the temperature dependence of the ESR signal of the spin probe in water prepared by the QRW and SC protocols, the former leading to ice with higher polycrystallinity. As usual, the lineshape, because of phase sensitive detection, is displayed in derivative mode by sweeping the magnetic field B_0 with constant microwave frequency ω ($\omega/2\pi \simeq$ 9.5 GHz in the present work).

Fig. 2 shows that, below about $210K$ the ESR lineshape of TEMPOL in the liquid fraction of the SC sample changes abruptly and one observes a broad peak due to the strong exchange and dipolar interactions between very close TEMPOL molecules clustered in liquid pockets with mutual distances less than ~ 2 nm [38,45,66–69].

This finding is consistent with the stronger water confinement in the SC sample than in the QRW sample – where the lineshape collapse was never observed – combined with the shrinkage of the reservoirs where TEMPOL is trapped when departing from the melting point [52,76].

Apart from the previous case, the ESR lineshapes in Fig. 2 are represented by three peaks. This pattern is characteristic of well

isolated nitroxide probe molecules in a liquid host with no mutual interactions [38,75]. The narrow width ($\sim$1 G) of each line of the triplet shown in Fig. 2 is due to the strong motional averaging of an otherwise broad ($\sim$70 G) inhomogeneous ESR line (motional narrowing in liquid, for details see refs. [38,75]). As a consequence, the *faster* the reorientation, the *narrower* the line. Inspection of Fig. 2 shows that TEMPOL rotates at comparable rates in SC and QRW liquid water at higher temperatures, whereas it becomes increasingly *faster* in SC water below T_m (compare the linewidths of the peaks, especially the rightmost one, of the ESR lineshape of TEMPOL in SC water at 210 K with the corresponding ones of the QRW water at the *higher* temperature 220 K). Due to the higher confinement of SC water with respect to QRW water, this finding is not trivial.

To gain more quantitative insight, we fitted the ESR lineshape of TEMPOL by using the numerical methods detailed elsewhere [38]. Due to the globular shape of TEMPOL, only *one* adjustable parameter describes its reorientation in a given environment *e*: the rotational correlation time τ_e, i.e. the area below the normalized time correlation function of the spherical harmonic $Y_{2,0}$. Roughly, τ_e is a measure of the average time needed by TEMPOL to overturn. The temperature dependence of the rotational correlation time τ_{SC} of TEMPOL in SC water is shown in Fig. 3 and compared to the one in QRW water, τ_{QRW} [38]. Before we go into the detailed comparison of τ_{SC} with the rich phenomenology of TEMPOL in QRW water, some preliminary remarks are in order. First, *no* signature of ice melting has been detected in QRW water while crossing T_m, or of water freezing in SC water between T_m and T_H. This is strong evidence that a negligible TEMPOL fraction is localized inside or close to the ice grains. Fig. 3 shows that the spin-probe reorientation in the supercooled region of QRW and SC water is strikingly different. The TEMPOL reorientation in SC water below T_m:

i) is *faster* than in QRW water (as hinted by Fig. 2),

ii) is driven by the *same* activated process as that of the equilibrium region ($T \gtrsim T_m$),

iii) does *not* show the signature of the fragile-to-strong dynamic crossover (FSC) temperature at $T_{FSC} \sim 228K$ which is seen in QRW water [77].

Since TEMPOL links up with the HB network of water [73], the above findings point to facilitated dynamics of the SC water with respect to QRW water. By reminding that SC water is more confined by the ice grains than QRW water, support to this conclusion is provided by the finding that the formation of unstrained hydrogen bonds, limiting the fluidity, is inhibited in restricted environments [42].

Energy and entropy barriers to TEMPOL reorientation

TEMPOL in QRW water between T_g and 180 K is embedded in two environments where it exhibits fast (F) and slow (S) mobilities, see Fig. 3 and also ref.[38]. The situation is sketched in Fig. 1a. Above 180 K the dynamical heterogeneity is averaged by the faster fluctuations and the ESR spectroscopy detects one *average* environment, denoted by FS (for simplicity labelled also as F in ref. [38]). It is intriguing to note that recent simulations of a monolayer of water adsorbed on a generic inert substrate evidence the disordering of the HB network above 180 K [78].

TEMPOL, which rotates by breaking and reforming hydrogen bonds with water molecules after jumps of about 60° [38,79], exhibits the same activation energy $\Delta E = 8.18$ kJ/mol in the slow fraction of QRW water, the SC water and the equilibrium region (Fig. 3). This compares well with the activation energy to switch hydrogen-bond partners in pure (7.7$-$8.37 kJ/mol [80]) and doped ($\sim$8.3 kJ/mol [81]) water. On this basis the TEMPOL reorientation is modeled as follows:

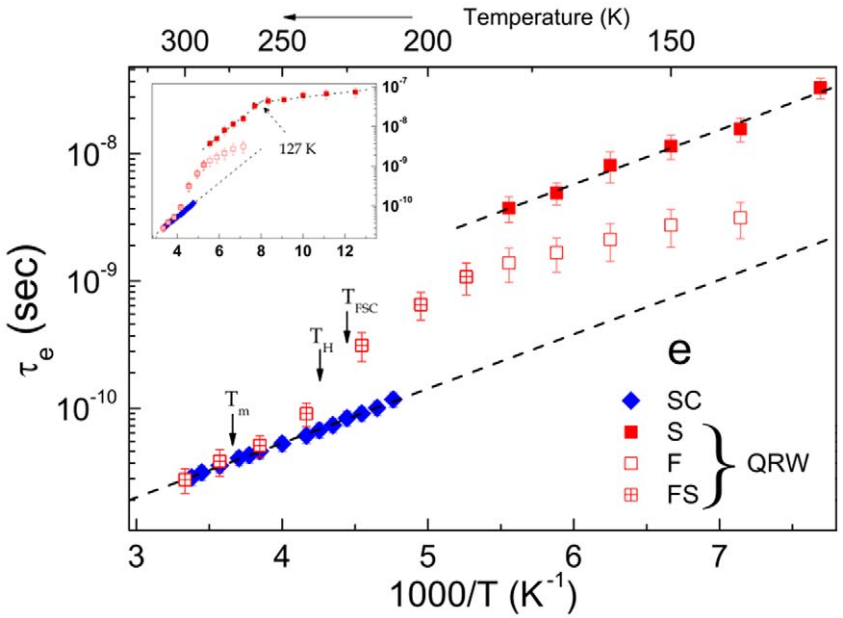

Figure 3. Rotational correlation time of TEMPOL in SC and QRW water. Part of the data are in the "no man's land" ($T_H > T > T_X$). The two *parallel* dashed lines with slope $\Delta E = 8.18$ kJ/mol are the Arrhenius best-fit of the correlation times of TEMPOL in equilibrium water, SC water (blue) and in the low-mobility S fraction of the QRW water (red). The inset plots the data including the sub-T_g region. Note: i) the change of regime at 127 K close to $T_g \simeq 136K$, ii) the absence of any abrupt change at T_m and, in SC water, at both T_H and T_{FSC}.
doi:10.1371/journal.pone.0044382.g003

i) TEMPOL switches water partner with an energy cost which is independent of both the water environment and the temperature.

ii) the additional temperature and environmental dependence of the reorientation rate is ascribed to the activation entropy $\Delta S_e(T)$ in the spirit of the transition-state theory.

We summarize the model by writing the TEMPOL reorientation time in a given environment e as:

$$\tau_e \propto \exp[-\Delta S_e(T)/R]\exp(\Delta E/RT) \quad (2)$$

with $\Delta E = 8.18$ kJ/mol and R the ideal gas constant. Fig. 3 shows that, if TEMPOL is in SC water ($e = $SC) or in the S fraction of the QRW water ($e = $S), the activation entropy is temperature independent. This is not the case in either F ($e = $F) or FS ($e = $FS) environments of QRW water.

To understand how entropy limits the reorientation of TEMPOL in QRW supercooled water, we focus on the entropic barrier increase with respect to equilibrium, $\delta\Delta S_e(T) \equiv \Delta S_{SC} - \Delta S_e(T)$, which is evaluated via Eq. 2 as:

$$\delta\Delta S_e(T) = R\ln[\tau_e(T)/\tau_{SC}(T)], \quad e = S,F,FS \quad (3)$$

Eq. 3 assumes that the temperature dependence of $\tau_{SC}(T)$ may be extrapolated below 210 K. The results concerning $\delta\Delta S_e(T)$ are shown in Fig. 4 and discussed below. Preliminarily, we define the quantity $\Delta S_m - S_{ex}(T)$ where S_{ex} and $\Delta S_m = 21.991 \pm 0.001$ J K^{-1} mol^{-1} are the thermodynamic estimate of the excess entropy of the liquid water over the crystal [82] and the entropy of melting [83], respectively. We also resorted to the very recent measurement $S_{ex}(150K) = 1.6 \pm 1$ J K^{-1} mol^{-1} [84]. $\Delta S_m - S_{ex}(T)$ is a measure of the number of water configurations lost on cooling from T_m to $T \le T_m$ as it is seen by the relation [82]:

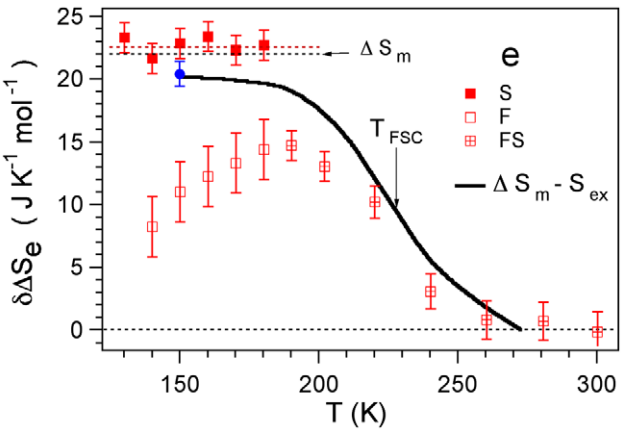

Figure 4. The entropy barrier to TEMPOL reorientation rising in supercooled QRW water. The dashed lines mark the entropy of melting $\Delta S_m = 21.991 \pm 0.001$ J K^{-1} mol^{-1} (black) and the best-fit value of the barrier of the slow fraction of TEMPOL $\delta\Delta S_S = 22.56 \pm 0.58$ J K^{-1} mol^{-1} (red). The solid black line is a measure of the number of water configurations lost on cooling from T_m to $T \le T_m$, $\Delta S_m - S_{ex}(T)$, where S_{ex} is the excess entropy of the liquid over the crystal [82]. The blue circle corresponds to $\Delta S_m - S_{ex}(150K) = 20.4 \pm 1$ J K^{-1} mol^{-1} [84].
doi:10.1371/journal.pone.0044382.g004

$$\Delta S_m - S_{ex}(T) = \int_T^{T_m} C_{ex}/T dT \quad (4)$$

where C_{ex} is the excess specific heat of the liquid water over the crystal.

High-temperature entropy barrier

First, we discuss the temperature range $T_{FSC} \le T \le T_m$. Fig. 4 shows that the increase of the activation entropy barrier $\delta\Delta S_e(T)$ and the number of configurations lost by water, $\Delta S_m - S_{ex}(T)$, are very close to each other from equilibrium down to the fragile-to-strong crossover at T_{FSC} [86]. From this, it is evidence that the entropic barrier to be surmounted by TEMPOL to switch water partner in the OH bond is largely controlled by the spatial arrangement of surrounding water molecules, and the latter is negligibly perturbed by the probe molecule. It is interesting to compare this finding, referred to the guest-host coupling, to the sharp linear correlation between the entropy barrier increase from T_m to T_g, $\delta\Delta S$, and the corresponding loss of the configurational entropy δS_{conf} observed in glassforming systems [85]. More specifically, if a molecule – linked to the surroundings by $\mathcal{P}$ bonds – rearranges with the participation of $Z^\star$ bonds, the approximate equality $\delta\Delta S \simeq Z^\star \delta S_{conf}/\mathcal{P}$ holds. In case of the hydrogen bonding between TEMPOL and water, by setting $\mathcal{P} = Z^\star = 1$ (see fig. 2) and by replacing T_g with a generic temperature T between T_g and T_m, one recovers our approximate equality between $\delta\Delta S_e(T)$ and $\Delta S_m - S_{ex}(T)$.

Low-temperature entropy barriers: ice-like regions in QRW water

We now discuss the temperature range $T_g \le T \le T_{FSC}$. Below 190 K ESR discriminates between the two TEMPOL fractions in the fast (F) and the slow (S) environments of QRW water, the latter with increasing weight on cooling [38] (the situation is sketched in Fig. 1a). From Eq. 3 ($e = S$) the entropic barrier of the S fraction is found to be constant, $\delta\Delta S_S = 22.56 \pm 0.58$ J K^{-1} mol^{-1} (Fig. 4). The fact that for $T \le 180$ K, $\Delta S_m - S_{ex}$ is lower than $\delta\Delta S_S$ is ascribed (at least in part) to the positive contribution to S_{ex} by less ordered environments.

$\delta\Delta S_S$ agrees with the entropy of melting ΔS_m within 2.6% ($\Delta S_m = 21.991 \pm 0.001$ J K^{-1} mol^{-1} [83]), i.e. the activation entropy of TEMPOL in equilibrium water ($T \gtrsim T_m$) exceeds its counterpart in the S fraction of supercooled water by the melting entropy. In addition to the observed near coincidence between the activation entropy of TEMPOL and the configurational entropy of its surrounding water between T_m and T_{FSC}, we take this finding as further evidence that water configurations control how TEMPOL switches from one hydrogen-bond water partner to another. More quantitatively, the present result is consistent with the conclusion that S liquid water maintains the fourfold coordination of ice within the ESR observation time $T_2^\star \sim 0.1\mu$s [38]. Elsewhere, we argued that the S environment is not solid [38].

Low-temperature entropy barriers: disordered regions in QRW water?

Below 190 K, ESR reveals a fast (F) environment of QRW water (see Fig. 3 and a sketch of the situation in Fig. 1a). The entropic barrier of the F fraction of TEMPOL $\delta\Delta S_F$ decreases by lowering the temperature (Fig. 4). The full characterization of the

F fraction is made problematic by the fact that the weight of the ESR signal of TEMPOL in the F fraction decreases on cooling [38]. However, if we insist on assuming that $\delta\Delta S_F$ is a measure of the configurational entropy, one speculates that the F fraction is less ordered than the S one, i.e. has higher entropy than the S fraction ($\Delta S_F > \Delta S_S$).

Lower limit of metastability of supercoooled water

Recent simulations of ice/water mixtures by Moore and Molinero evidenced the presence of threads and clusters of water molecules with local structure intermediate between ice I and liquid [29,62]. This form of water, called intermediate ice [29], is thought to be a constitutive part of the structure of water at 180 K [62]. At the beginning of the crystallization process the intermediate ice is already present and unrelated to crystal cores, whereas it localizes on the surface of ice crystallites at later stages. The major conclusion of ref. [29] is that the rate and mechanisms of ice formation is controlled by structural transformation leading to a sharp increase in the fraction of four-coordinated molecules in supercooled liquid water. An interesting consequence is that below $T_x \sim 225$ K (from classical nucleation theory) or ~ 202 K (from numerical simulation) ice nuclei form faster than liquid water can equilibrate, i.e. water is not in a metastable state but is *out-of-equilibrium*. Said otherwise, T_x sets an effective lower limit of metastability of supercoooled water. Then, it is argued that in the range $T_g < T < T_x$ there is no metastable liquid water, but rather a less viscous liquid unable to relax before crystallizing [29].

Our experimental results, and their interpretation, put constraints to the above scenario. We reached temperatures lower than T_x by the QRW protocol, i.e. quench-cooling to a state below T_g which is bound to be out-of equilibrium and then rewarming to the temperature of interest. Fig. 4 shows that the local structure of the S fraction of QRW water surrounding TEMPOL in the range $130-180$ K is well equilibrated and close to ice. We remind that TEMPOL is *not* trapped in solid-state ice [38,45,58,60,66–69]. More experimental and numerical work is needed to clarify the matter. In particular we notice that the water model used in ref. [29] is a coarse-grained, monatomic model. It proved exceedingly useful and insightful in the investigation of several aspects of supercooled water's thermodynamics. However, the dynamics of this model is faster than in actual water because the barrier for breaking the hydrogen bonds is underestimated [62]. This barrier is involved in the mobility of water and the rate of crystallization. Then, the subtle interplay of crystallization dynamics and relaxation dynamics in the supercooled liquid could be not reproduced optimally in this model.

Conclusion

In conclusion, we investigated the rotational dynamics of a probe molecule localized in the interstitial supercooled water of polycrystalline ice. The degree of confinement of the liquid water was found to vary according to the polycrystallinity of the ice. It is observed that the probe molecule has higher rotational mobility in water with stronger confinement. We interpret the probe dynamics in terms of a simple activated process with constant activation energy, due to probe's hydrogen bonding with water, and a suitable entropy barrier. We argue that the entropy barrier, which is due – through hydrogen bonding – to the configuration of the surrounding water molecules, yields a direct measure of the configurational entropy of the same. We find that, under loose confinement on supercooled water, the entropy barrier surmounted by the slower probe fraction exceeds that of equilibrium water by the melting entropy of ice, whereas no increase of the barrier is observed under stronger confinement. We conclude that loose confinement allows the presence of ice-like regions in supercooled water, whereas a tighter confinement yields the suppression of the water ordered fraction and leads to higher fluidity. Our results point to the striking conclusion that strengthening the confinement of water by ice destabilizes the hydrogen bond network of the liquid, even if one anticipates strong ordering induced by ice on water. These findings have broad implications on biology, atmospheric phenomena, geology, food technology as well as fundamental physics. In particular, they put constraints to recent numerical studies of the lower limit of metastability of supercoooled water.

Materials and Methods

Samples were prepared in a capillary (dia $\sim 100\mu m$) by doping a small amount of triple distilled water with about 0.1% by weight of the polar radical TEMPOL (spin probe). TEMPOL accommodates well in water due to hydrogen-bonds and the moderate size ($r_{TEMPOL} \sim 0.34 nm$ to be compared to $r_{H2O} \sim 0.14 nm$).

The amorphous water samples (QRW protocol) were prepared by direct exposition to liquid helium ($4.2K$) *in situ* in the ESR low temperature cryostat. The liquid helium transfer tube was modified such that a burst of liquid helium hits the capillary cooling it to $4.2K$ almost instantaneously leading to the formation of vitrified water.

The ESR signal of TEMPOL are recorded by using a X-band Bruker ER 200 CW EPR spectrometer. At a selected temperature no aging, i.e. no sample evolution, was ever detected.

The lineshape is evaluated by a stochastic memory-function approach [87,88]. The reorientation of TEMPOL, due to its globular shape, is modeled by instantaneous random jumps with fixed size θ after a mean residence time τ_0 [89], as validated by theory [90] and simulations [91]. Under this hypothesis, the rotational correlation time τ (the area below the normalized correlation function of the spherical harmonic $Y_{2,0}$ [75]) is given by $\tau = \tau_0/[1 - \sin(5\theta/2)/5\sin(\theta/2)]^{-1}$. The temperature-independent magnetic parameters of TEMPOL were determined by the rigid-limit lineshape recorded at low temperature – where angular displacements are small [92–99] – according to a procedure detailed elsewhere [100].

The number of adjustable parameters of the theoretical lineshape changes over the temperature range under investigation. In general, the ESR lineshape of TEMPOL in QRW water is fitted by using two components, corresponding to the fast (F) and slow (S) fractions of TEMPOL, with weights w_f and $w_s = 1 - w_f$, respectively. The S component depends on two adjustable parameters, i.e. τ_S and θ_S, whereas, due to rapid motion, the F component depends on τ_F only. Therefore, to fit the ESR lineshape in the temperature region $140-180K$ one needs four adjustable parameters ($\tau_S, \theta_S, \tau_F, w_F$). These reduce to two ($\tau_S, \theta_S$) at lower temperatures where $w_s \simeq 1$ and one ($\tau_{FS} \equiv \tau_F$) to higher temperatures where $w_f \simeq 1$. For TEMPOL in SC water only one fitting parameter (τ_{SC}) is needed. The theoretical lineshape was convoluted by a gaussian curve with width $1/T_2^\star$ to account for the magnetic field produced by the rotating methyl groups close to the unpaired electron. $T_2^\star$ increases with the temperature from ~ 30 ns up to ~ 40 ns in the temperature range $90K-300K$.

Acknowledgments

DL thanks S. Capaccioli, G. Carini, F. Mallamace, C. A. Massa, L. Pardi, A. Rizzo, S. N. Shore and E. Tombari for comments and helpful discussions. DB thanks Jayanta Parui and Tridib Sadhu for several discussions.

Author Contributions

Analyzed the data: DB SVB DL. Wrote the paper: DL. Designed research: SVB DL. Performed research: DB SNB SVB DL. Interpreted the results: DL. Refined the manuscript: DB SVB.

References

1. Stillinger FH (1980) Water Revisited. Science 209: 451–457.
2. Mishima O, Stanley HE (1998) The relation between liquid, supercooled and glassy water. Nature 396: 329–335.
3. Debenedetti PG (2003) Supercooled and glassy water. J. Phys.: Condens. Matter 15: R1669–R1726.
4. Angell CA (2008) Insights into Phases of Liquid Water from Study of Its Unusual Glass-Forming Properties. Science 319: 582–587.
5. Soper AK (2008) Structural transformations in amorphous ice and supercooled water and their relevance to the phase diagram of water. Mol Phys 106:2053–2076.
6. Brovchenko I, Oleinikova A (2008) Multiple Phases of Liquid Water. Chem Phys Chem 9: 26602675.
7. Huang C, Wikfeldt KT, Tokushima T, Nordlund D, Harada Y, et al. (2009) The inhomogeneous structure of water at ambient conditions. Proc Natl Acad Sci USA 106: 15214–15218.
8. Clark GNI, Hura GL, Teixeira J, Soper AK, Head-Gordon T (2010) Small-angle scattering and the structure of ambient liquid water. Proc Natl Acad Sci USA 107: 14003–14007.
9. Clark GNI, Cappa CD, Smith JD, Saykally RJ, Head-Gordon T (2010) The structure of ambient water. Mol Phys 108: 1415–1433.
10. Eisenberg D, Kauzmann W (1969) The Structure and Properties of Water (Oxford University Press, London, UK).
11. Whiting H (1884) A Theory of Cohesion (Harvard University, Cambridge, USA).
12. Frank HS, Wen W-Y (1957) Ion-solvent interaction. Structural aspects of ion-solvent interaction in aqueous solutions: a suggested picture of water structure. Discuss Faraday Soc 24:133–140.
13. Nemethy G, Scheraga HA (1962) Structure of Water and Hydrophobic Bonding in Proteins. I. A Model for the Thermodynamic Properties of Liquid Water. J Chem Phys36: 3382–3400.
14. Bernal JD, Fowler RH (1933) A Theory of Water and Ionic Solution, with Particular Reference to Hydrogen and Hydroxyl Ions. J Chem Phys1: 515–548.
15. Pople JA (1951) Molecular Association in Liquids. II. A Theory of the Structure of Water. Proc Roy Soc of London Ser A, Math Phys 205: 163–178.
16. Stillinger FH (1980) Thermal Properties of Water in Restrictive Geometries, in "Water in Polymers", S. P. Rowland, Ed. (American Chemical Society, Washington, D.C.).
17. Moore EB, Molinero V (2009) Growing correlation length in supercooled water. J Chem Phys 130: 244505.
18. Mishima O, Calvert LD, Whalley E (1985) An apparently first-order transition between two amorphous phases of ice induced by pressure. Nature 314: 76–78.
19. Poole PH, Sciortino F, Essmann U, Stanley HE (1992) Phase behaviour of metastable water. Nature 360: 324–328.
20. Tanaka H (2000) General view of a liquid-liquid phase transition. Phys Rev E 62: 6968–6976.
21. Tanaka H (2000) Simple physical model of liquid water. J Chem Phys 112: 799–809.
22. Speedy RJ (1982) Limiting forms of the thermodynamic divergences at the conjectured stability limits in superheated and supercooled water. J Phys Chem 86:3002–3005.
23. Stanley HE, Teixeira J (1980) Interpretation of the unusual behavior of H_2O and D_2O at low temperatures: Tests of a percolation model. J Chem Phys 73: 3404–3422.
24. Sastry S, Debenedetti PG, Sciortino F, Stanley HE (1996) Singularity-free interpretation of the thermodynamics of supercooled water. Phys Rev E 53:6144–6154.
25. Borick SS, Debenedetti PG, Sastry S (1995) A lattice model of network-forming fluids with orientation-dependent bonding: Equilibrium, stability, and implications for the phase-behavior of supercooled water. J Phys Chem 99:3781–3792.
26. Poole PH, Sciortino F, Grande T, Stanley HE, Angell CA (1994) Effect of hydrogen bonds on the thermodynamic behavior of liquid water. Phys Rev Lett 73:1632–1635.
27. Stokely K, Mazza MG, Stanley HE, Franzese G (2010) Effect of hydrogen bond cooperativity on the behavior of water. Proc Natl Acad Sci USA 107: 1301–1306.
28. Errington JR, Debenedetti PG, Torquato S (2002) Cooperative Origin of Low-Density Domains in Liquid Water. Phys Rev Lett 89: 215503.
29. Moore EB, Molinero V (2011) Structural transformation in supercooled water controls the crystallization rate of ice. Nature 479: 506–509.
30. Kumar P, Buldyrev SV, Stanley HE (2009) A tetrahedral entropy for water. Proc Natl Acad Sci USA 106: 22130–22134.
31. Wikfeldt KT, Nilsson A, Pettersson LGM (2011) Spatially inhomogeneous bimodal inherent structure of simulated liquid water. Phys Chem Chem Phys 13: 19918–19924.
32. Mishima O, Stanley HE (1998) Decompression-induced melting of ice IV and the liquid-liquid transition in water. Nature 392:164–168.
33. Soper AK, Ricci MA (2000) Structures of High-Density and Low-Density Water Phys Rev Lett. 84: 2881–2884.
34. Mallamace F, Corsaro C, Broccio M, Branca C, Gonzalez-Segredo N, et al. (2008) NMR evidence of a sharp change in a measure of local order in deeply supercooled confined water. Proc Natl Acad Sci USA 105: 12725–12729.
35. Kim CU, Barstow B, Tate MW, Gruner SM (2009) Evidence for liquid water during the highdensity to low-density amorphous ice transition. Proc Natl Acad Sci USA 106:4596–4600.
36. Mallamace F, Broccio M, Corsaro C, Faraone A, Majolino D, et al. (2007) Evidence of the existence of the low-density liquid phase in supercooled, confined water. Proc Natl Acad Sci USA 104: 424–428.
37. Bosio L, Stanley HE, Teixeira J (1981) Enhanced Density Fluctuations in Supercooled H_2O, D_2O, and Ethanol-Water Solutions: Evidence from Small-Angle X-Ray Scattering. Phys Rev Lett 46: 597–600.
38. Banerjee D, Bhat SN, Bhat SV, Leporini D (2009) ESR evidence for 2 coexisting liquid phases in deeply supercooled bulk water. Proc Natl Acad Sci USA 106:11448–11453.
39. Zhang Y, Faraone A, Kamitakahara WA, Liu KH, Mou CY, et al. (2011) Density hysteresis of heavy water confined in a nanoporous silica matrix. Proc Natl Acad Sci USA 108: 12206–12211.
40. Tulk CA, Benmore CJ, Urquidi J, Klug DD, Neuefeind J, et al. (2002) Structural studies of several distinct metastable forms of amorphous ice. Science 297:1320–1323.
41. Matsumoto M (2009) Why Does Water Expand When It Cools? Phys. Rev. Lett. 103: 017801.
42. Raviv U, Laurat P, Klein J (2001) Fluidity of water confined to subnanometre films. Nature 413: 51–54.
43. Malani A, Ayappa KG, Murad S (2009) Influence of hydrophilic surface specificity on the structural properties of confined water. J Phys Chem B 113:13825–13839.
44. Gallo P, Rovere M, Chen S-H (2010) Dynamic crossover in supercooled confined water: Understanding bulk properties through confinement. J Phys Chem Lett 1:729–733.
45. Bhat SN, Sharma A, Bhat SV (2005) Vitrification and Glass Transition of Water; Insights from Spin Probe ESR. Phys Rev Lett 95: 235702.
46. Capaccioli S, Ngai KL (2011) Resolving the controversy on the glass transition temperature of water ?. J Chem Phys 135: 104504.
47. Rosenhain W, Ewen D (1913) The intercrystalline cohesion of metals. J Inst Metals 10: 119–148.
48. Zhang H, Srolovitz DJ, Douglas JF, Warren JA (2009) Grain boundaries exhibit the dynamics of glass-forming liquids. Proc Natl Acad Sci USA 106:7735–7740.
49. Nye JF, Frank FC (1973) Hydrology of the intergranular veins in a temperate glacier. International Association of Scientific Hydrology Publication 95 (Symposium at Cambridge 1969 – *Hydrology of Glaciers*), 157–161.
50. Nye JF (1991) Thermal behaviour of glacier and laboratory ice. J Glaciology 37: 401–413.
51. Mader HM (1992) Observations of the water-vein system in polycrystalline ice. J Glaciology 38: 333–347.
52. Mader HM (1992) The thermal behaviour of the water-vein system in polycrystalline ice. J Glaciology 38: 359–374.
53. Dowell LG, Rinfret AP (1960) Low-temperature forms of ice as studied by X-ray diffraction. Nature 188: 1144–1148.
54. Jenniskens P, Blake DF (1994) Structural Transitions in Amorphous Water Ice and Astrophysical Implications. Science 265: 753–756.
55. Jenniskens P, Blake DF (1996) Crystallization of amorphous water ice in the solar system. Astrophys. J. 473:1104–1113.
56. Jenniskens P, Banham SF, Blake DF, McCoustra MRS (1997) Liquid water in the domain of cubic crystalline ice *Ic*. J Chem Phys. 107: 1232–1241.
57. Souda R (2007) Two Liquid Phases of Water in the Deeply Supercooled Region and Their Roles in Crystallization and Formation of LiCl Solution. J Phys Chem B 111: 5628–5634.
58. Johari GP (1995) Obtaining further information from calorimetry. Thermochim Acta 266: 31–47.
59. Johari GP, Pascheto W, Jones SJ (1994) Intergranular liquid in solids and premelting of ice. J Chem Phys.100: 4548–4553.
60. Johari GP (1998) Thermodynamics of water-cubic ice and other liquid-solid coexistence in nanometer-size particles. J Chem Phys.109: 1070–1073.
61. Xiaoshuang S, Chen L, Li D, Zhu L, Wang H, et al. (2011) Assembly of Colloidal Nanoparticles Directed by the Microstructures of Polycrystalline Ice. ACS Nano 5: 8426–8433.
62. Moore EB, Molinero V (2010) Ice crystallization in water's "no man's land". J Chem Phys 132: 244504.

63. Barnes PRF, Wolff EW, Mallard DC, Mader HM (2003) SEM Studies of the Morphology and Chemistry of Polar Ice. Microsc Res Tech 62: 62–69.
64. Salvetti G, Tombari E, Johari GP (1995) Calorimetric effects of intergranular water in ice. J Chem Phys 102: 4987–4990.
65. Pruppacher HR (1967) On the growth of ice crystals in supercooled water and aqueous solution drops. Pure and Applied Geophys. 68: 186–195.
66. Ross RT (1965) Dipolar broadening of EPR spectra due to solute segregation in frozen aqueous solution. J Chem Phys 42: 3919–3922.
67. Leigh JS Jr, Reed GH (1971) Electron paramagnetic resonance studies in frozen aqueous solutions. Elimination of freezing artifacts. J. Phys. Chem. 75: 1202–1204.
68. Ahn M-K (1976) Electron spin relaxation of di-tertiary-butyl nitroxide in supercooled water. J Chem Phys 64,: 134–138.
69. Santangelo MG, Levantino M, Cupane A, Jeschke G (2008) Solvation of a Probe Molecule by Fluid Supercooled Water in a Hydrogel at 200 K. J Phys Chem B 112: 15546–15553.
70. Frank FC (1968) Two-component flow model for convection in the Earth's upper mantle. Nature 220: 350–352.
71. Brice JC (1973) The Growth of Crystals from Liquids (North-Holland, Amsterdam, The Netherlands).
72. De los Santos F, Franzese G (2012) Relations between the diffusion anomaly and cooperative rearranging regions in a hydrophobically nanoconfined water monolayer. Phys Rev E 85: 010602(R).
73. Houriez C, Masella M, Ferré N (2010) Structural and atoms-in-molecules analysis of hydrogen-bond network around nitroxides in liquid water. J Chem Phys 133: 124508.
74. Weil JA, Bolton JR (2006) Electron Paramagnetic Resonance: Elementary Theory and Practical Applications (Wiley-Interscience, New York, USA).
75. Nordio PL (1976) in Spin labeling: theory and applications, ed Berliner LJ (Academic Press, New York, USA), 5–52.
76. Wettlaufer JS, Grae Worster M (2006) Premelting Dynamics. Annu Rev Fluid Mech 38: 427–452.
77. Ito K, Moynihan CT, Angell CA (1999) Thermodynamic determination of fragility in liquids and a fragile-to-strong liquid transition in water. Nature 398: 492–495.
78. Mazza MG, Stokely K, Pagnotta SE, Bruni F, Stanley HE, et al. (2011) More than one dynamic crossover in protein hydration water. Proc Natl Acad Sci USA 108: 19873–19878.
79. Laage D, Hynes JT (2006) A Molecular Jump Mechanism of Water Reorientation. Science 311: 832–835.
80. Smith JD, Cappa CD, Wilson KR, Cohen RC, Geissler PL, et al. (2005) Unified description of temperature-dependent hydrogen-bond rearrangements in liquid water. Proc Natl Acad Sci USA 102: 14171–14174.
81. Alavi S, Susilo R, Ripmeester JA (2009) Linking microscopic guest properties to macroscopic observables in clathrate hydrates: Guest-host hydrogen bonding. J Chem Phys 130: 174501.
82. Starr FW, Angell CA, Stanley HE (2003) Prediction of entropy and dynamic properties of water below the homogeneous nucleation temperature. Physica A 323: 51–66.
83. Feistel R, Wagner WA (2006) New Equation of State for H_2O Ice Ih. J Phys Chem Ref Data 35: 1021–1047.
84. Scott Smith R, Matthiesen J, Knox J, Kay BD (2011) Crystallization Kinetics and Excess Free Energy of H_2O and D_2O Nanoscale Films of Amorphous Solid Water. J Phys Chem A 115: 5908–5917.
85. Nemilov SV (2007) Structural aspect of possible interrelation between fragility (length) of glass forming melts and Poissons ratio of glasses. J Non-Cryst Solids 353: 4613–4632.
86. Chen S-H, Mallamace F, Mou C-Y, Broccio M, Corsaro C, et al. (2006) The violation of the Stokes-Einstein relation in supercooled water. Proc Natl Acad Sci USA 103: 12974–12978.
87. GiordanoM, Grigolini P, Leporini D, Marin P (1983) Fast computational approach to the evaluation of slow motion EPR spectra in terms of a generalized Langevin equation. Phys. Rev. A 28: 2474–2481.
88. Leporini D (1994), Relationship between a nonlinear response and relaxation induced by colored noise. Phys. Rev. *A* 49: 992–1014.
89. Andreozzi L, Cianflone F, Donati C, Leporini D (1996) Jump reorientation of a molecular probe in the glass transition region of o-terphenyl. J. Phys.: Condens. Matter 8: 3795–3809.
90. Douglas JF, Leporini D (1998) Obstruction Model of the Fractional Stokes-Einstein Relation in Glass-forming liquids. J Non-Cryst Solids 235–237: 137–141.
91. De Michele C, Leporini D (2001) Viscous flow and jump dynamics in Molecular Supercooled Liquids. II. Rotations. Phys Rev E 63: 036702.
92. Larini L, Ottochian A, De Michele C, Leporini D (2008) Universal scaling between structural relaxation and vibrational dynamics in glass-forming liquids and polymers. Nature Phys 4: 42–45.
93. Ottochian A, De Michele C, Leporini D (2009) Universal divergenceless scaling between structural relaxation and caged dynamics in glass-forming systems. J Chem Phys. 131: 224517.
94. Ottochian A, Leporini D (2011) Universal scaling between structural relaxation and caged dynamics in glass-forming systems: free volume and time scales. J Non-Cryst Solids 357, 298–301.
95. Ottochian A, Leporini D (2011) Scaling between structural relaxation and caged dynamics in $Ca_{0.4}K_{0.6}(NO_3)_{1.4}$ and glycerol: Free volume, time-scales and implications for pressure-energy correlations. Phil Mag 91: 1786–1795.
96. De Michele C, Del Gado E, Leporini D (2011) Scaling between structural relaxation and particle caging in a model colloidal gel. *Soft Matter* 7: 4025–4031.
97. Puosi F, Leporini D (2012) Spatial displacement correlations in polymeric systems. J Chem Phys. 136: 164901.
98. Puosi F, Leporini D (2011) Scaling between relaxation, transport, and caged dynamics in polymers: from cage restructuring to diffusion. J. Phys. Chem. *B* 115: 14046–14051.
99. Barbieri A, Campani E, Capaccioli S, Leporini D (2004) Molecular dynamics study of the thermal and the density effects on the local and the large-scale motion of polymer melts: Scaling properties and dielectric relaxation. J Chem Phys 120: 437–453.
100. Andreozzi L, Giordano M, Leporini D (1993) Efficient characterization of the orientational ordering of ESR-active probes in supermolecular fluids. Appl. Magn. Reson. 4: 279–295.